Mineralogy and geochemistry of trace elements in bauxites: The Devonian Schugorsk deposit, Russia

Article *in* Mineralogical Magazine · February 2001

DOI: 10.1180/002646101550145

3 authors, including:

Christopher J Stanley
Natural History Museum, London
248 PUBLICATIONS **2,396** CITATIONS

SEE PROFILE

Mineralogical Magazine, February 2001, Vol. 65(1), pp. 81–101

Mineralogy and geochemistry of trace elements in bauxites: the Devonian Schugorsk deposit, Russia

L. E. MORDBERG[1,2,3], C. J. STANLEY[2] AND K. GERMANN[3]

[1] Russian Research Geological Institute (VSEGEI), Sredny pr 74, St. Petersburg, Russia
[2] The Natural History Museum, Cromwell Road, London SW7 5BD, UK
[3] Technische Universität Berlin, Lagerstättenforschung, Sekr. BH4, Ernst-Reuter-Platz 1, 10587 Berlin, Germany

ABSTRACT

Processes of mineral alteration involving the mobilization and deposition of more than 30 chemical elements during bauxite formation and epigenesis have been studied on specimens from the Devonian Schugorsk bauxite deposit, Timan, Russia. Chemical analyses of the minerals were obtained by electron microprobe and element distribution in the minerals was studied by element mapping. Interpretation of these data also utilized high-resolution BSE and SE images.

The main rock-forming minerals of the Vendian parent rock are calcite, dolomite, feldspar, aegirine, riebeckite, mica, chlorite and quartz; accessory minerals are pyrite, galena, apatite, ilmenite, monazite, xenotime, zircon, columbite, pyrochlore, chromite, bastnaesite and some others. Typically, the grain-size of the accessory minerals in both parent rock and bauxite is from 1 to 40 μm. However, even within these rather small grains, the processes of crystal growth and alteration during weathering can be determined from the zonal distribution of the elements. The most widespread processes observed are: (1) Decomposition of Ti-bearing minerals such as ilmenite, aegirine and riebeckite with the formation of 'leucoxene', which is the main concentrator of Nb, Cr, V and W. Crystal growth can be traced from the zonal distribution of Nb (up to 16 wt.%). Vein-like 'leucoxene' is also observed in association with organics. (2) Weathering of columbite and pyrochlore: the source of Nb in 'leucoxene' is now strongly weathered columbite, while the alteration of pyrochlore is expressed in the growth of plumbopyrochlore rims around Ca-rich cores. (3) Dissolution of sulphide minerals and apatite and the formation of crandallite group minerals: 'crandallite' crystals of up to 40 μm size show a very clear zonation. From the core to the rim of a crystal, the following sequence of elements is observed: Ca → Ba → Ce → Pb → Sr → Nd. Sulphur also shows a zoned but more complicated distribution, while the distribution of Fe is rather variable. A possible source of *REE* is bastnaesite from the parent rock. More than twelve crandallite type cells can be identified in a single 'crandallite' grain. (4) Alteration of stoichiometric zircon and xenotime with the formation of metamict solid solution of zircon and xenotime: altered zircon rims also bear large amounts of Sc (up to 3.5 wt.%), Fe, Ca and Al in the form of as yet unidentified inclusions of 1–2 μm. Monazite seems to be the least altered mineral of the profile.

In the parent rock, an unknown mineral of the composition (wt.%): ThO_2 – 54.8; FeO – 14.6; Y_2O_5 – 2.3; CaO – 2.0; *REE* – 1.8; SiO_2 – 12.2; P_2O_5 – 2.8; total – 94.2 (average from ten analyses) was determined. In bauxite, another mineral was found, which has the composition (wt.%): ThO_2 – 24.9; FeO – 20.5; Y_2O_5 – 6.7; CaO – 2.0; ZrO – 17.6; SiO_2 – 8.8; P_2O_5 – 5.4; total – 89.3 (F was not analysed; average from nine analyses). Presumably, the second mineral is the result of weathering of the first one. Although the Th content is very high, the mineral is almost free of Pb. However, intergrowths of galena and pyrite are observed around the partially decomposed crystals of the mineral. Another generation of galena is enriched in chalcophile elements such as Cu, Cd, Bi etc., and is related to epigenetic alteration of the profile, as are secondary apatite and muscovite.

KEYWORDS: bauxite, laterite, weathering, geochemistry, mineralogy, trace elements, leucoxene, crandallite, zircon, xenotime, pyrochlore, galena.

* E-mail: c.stanley@nhm.ac.uk

Introduction

THE problem of trace elements in bauxite profiles is important for a number of reasons. Firstly, deep chemical weathering is a geochemical process which is as important as magmatism, metamorphism or sedimentation. In addition, principles of concentration and/or differentiation of chemical elements during bauxite formation differ from those typical for magmatic, metamorphic and sedimentary processes. Secondly, only a few elements such as Ga and V are successfully extracted as by-products of Al production, although some other elements may show high concentrations within bauxite profiles. Thus, the nature of the minerals containing trace elements is an important key for the understanding of their behaviour during bauxite formation.

The problem of mobility of chemical elements during deep weathering has been discussed for many years. However, the very small grain-size of bauxite (a few microns or even smaller) has hindered detailed investigations. The most widespread method used to determine element mobility was a comparison of its bulk content in the parent rock and in the weathering profile, frequently using isovolumetric calculations. Bárdossy and Aleva (1990) compared data on six bauxite districts and concluded that "there exist a number of elements for which their chemical properties unequivocally determine enrichment or depletion in all lateritic-bauxite districts" (p. 145). This conclusion needs explanation.

This study on the mineralogy and geochemistry of trace elements in bauxite was carried out on samples from the Schugorsk bauxite deposit from the Middle Timan, Russia. Material from this deposit contains higher levels of certain elements than normal (Mordberg, 1996, 1997) and is hence suitable for a detailed mineralogical investigation.

Geology

Bauxite deposits of the Middle Timan are located in the North of European Russia, between the NE edge of the Russian Plate and the Pechorsk Depression (Fig. 1). The geology of the bauxite region has been given in detail by Likhachev (1993) and Mordberg (1996, 1997). Devonian bauxite deposits located within the Chetlass orogenic structure occur on folded, mostly carbonate strata of the Riphean. Deposits of both lateritic and karstic origin are found. The overlying rocks are Upper Devonian volcanogenic and sedimentary sequences; in some instances the bauxite profile is covered directly by Late Devonian trap basalt.

The Schugorsk bauxite deposit, the largest in the region, was formed over a Precambrian carbonate sequence which had been altered by alkali metasomatic processes. Rock-forming minerals of the metasomatite are dolomite, calcite and K-feldspars. Plagioclase, aegerine, riebeckite, biotite and 'sericite' are also present in various amounts. The weathered profile attains a total depth here of 100–120 m, and the main ore-forming minerals are boehmite, kaolinite and hematite with nearly monomineralic white boehmitic bauxites being widespread within the deposit. The ratio of carbonate and silicate minerals in the parent rock varies broadly with

FIG. 1. Location of the study area.

an average of ~1:1. Due to this heterogeneity, the deposit cannot be treated as either the lateritic or the karstic type.

Material and methods

Samples for the investigation were taken from drill cores. A part of each sample was powdered, and the levels present of 60 elements (including the major ones) were determined by XRF following standard methods at the Technical University of Berlin. A full description of the methods is given by Krumb (1998). The contents of elements in minerals were determined in polished sections using a wavlength-dispersive (WD) electron probe microanalyser (Cameca SX50) at the Natural History Museum, London. International standards were used for calibration of each element. The analytical conditions used were 15 kV and 20 nA with counting times of 20 s for Zr, Ca, Ti, Nb, P, Sc, Pb, Mn, Fe, Hf, Na, Mg, Al and Si; of 30 s for La, Ce, Th, U, Pb and W; and of 50 s for Y, Pr, Nd, Sm and Dy. Elemental X-ray maps were obtained using the following conditions: 15 kV, 100 nA and 200 μS per point.

Results

Rock geochemistry

The distribution parameters of Ti, P, S and trace elements within the Schugorsk weathering profile are given in Table 1. For comparison, data for the average composition of bauxite deposits of the world (Bronevoy *et al*., 1985) are also supplied. It can be seen that the studied profile is strongly enriched in lithophile elements such as Nb, Th, *REE* and Zr which are typical of alkali rocks. Chalcophile elements such as Pb, Sb, Bi and presumably Cd are also prominent, and the enrichment in W and Tl is of great interest also. The other elements which are found in amounts greater than average for bauxite are Ti, P, Ga, Ni, Sc, Sn, Sr and Zn. Some elements such as Ag, Co, U and V show concentrations close to average, while S, As, Cr, Cu and Hf occur in relatively small amounts. Both Zr/Hf (47.2) and Th/U (17.5) are much higher than their average values for bauxite.

Correlation analysis of element contents (Table 2) allows at least three groups of elements to be distinguished with high positive links among elements within each group. One group unites P, Ba, Sr, Bi and V; the other elements having a positive correlation with some of these are Ni and Pb. This group represents 'crandallite' mineralization within the profile. The second group consists of *REE* (La, Sm, Nd, Pr and Ce) with adjusted Y and, to a lesser extent, U. It reflects the presence of P-minerals such as monazite and xenotime. From these two groups, only Pb and Ce correlate positively with each other, both correlating with Cr and Sc as well. The third group represents Ti, Zr, Hf and Nb and reflects the presence of minerals such as 'leucoxene', zircon, columbite and pyrochlore. Elements without any high positive correlation are Th (due to its own mineral form), Ga (presumably dispersed in boehmite) and Zn (host minerals are unidentified). Elements determined in selected samples or with concentrations below the detection limit were excluded from the correlation analysis.

Mineralogy

The parent rock is composed of calcite and dolomite (sedimentary and diagenetic minerals), K-feldspars, aegirine and riebeckite (metasomatic minerals) and some micas, chlorite and quartz (terrigenous admixture). Ilmenite, monazite, xenotime, zircon, apatite, columbite, pyrochlore, pyrite, galena, sphalerite and some minerals such as bastnaesite and thorianite represent accessory minerals. The rock-forming minerals all completely disappeared during bauxite formation, but they may occur near the bottom of the weathering profile. The main minerals of bauxite are boehmite, hematite and kaolinite. Illite occurs in the less altered zones of the profile. Hydrothermal muscovite veins cross the profile. Accessory minerals of the profile are described below.

'Leucoxene'

Titanium oxide minerals are quite common in bauxite profiles of different origin. Anatase is the most widespread and it has been identified in many karst and laterite deposits (Bárdossy, 1982; Bárdossy and Aleva, 1990). Within the studied profile, Ti-oxides are not distinguished in detail; they are referred to as 'leucoxene'. However, from previous works (Likhachev, 1993), it is known that the main Ti mineral is anatase, and that rutile is also present. Typically, the crystal size varies from 1 to 40−50 μm, sometimes up to a few hundred μm. 'Leucoxene' often contains Nb (up to 20 wt.% of Nb_2O_5), Fe, W and Cr (Table 3). All the elements show a clear zonal distribution which can be seen in the X-ray maps (Figs 2, 3). On the back scattered electron image

TABLE 1. Chemical composition of bauxite profile (XRF data).

Element		Mean	Median	Mode	S.D.	Min	Max	*n*	AB
TiO_2	wt.%	3.47	3.84	1.74	1.32	0.82	6.03	51	2.25
P_2O_5		0.50	0.44	0.64	0.36	0.05	1.78	51	0.26
SO_3		0.05	0.05	0.05	0.04	0.01	0.21	27	0.17
Ag	ppm	4	3	3	4	0	21	27	4
As		13	10	7	11	2	67	50	48
Ba		255	148	297	347	32	2300	51	n.g.
Bi		18	16	13	10	7	64	51	0.9
Cd		13	12	12	9	1	46	27	n.g.
Co		20	16	4	18	0	74	51	18
Cr		233	247	168	111	74	651	51	420
Cu		18	11	4	26	0	159	51	28
Ga		98	104	101	37	9	162	51	71
Hg		1	1	1	1	1	7	27	n.g.
Hf		17	17	17	6	5	30	51	27
Mo		3	3	2	2	0	6	27	n.g.
Nb		513	425	371	324	20	1519	51	45
Ni		63	28	12	76	7	408	51	29
Pb		543	360	9	607	6	2371	51	48
Sb		19	16	17	17	9	100	27	2.4
Sc		82	68	100	54	12	307	51	25
Sn		28	28	27	10	4	51	27	10
Sr		900	709	485	797	18	3959	51	300
Th		155	150	150	105	12	535	51	30
Tl		11	12	13	4	1	19	27	0.1
U		9	10	11	4	0	16	51	6
V		318	223	216	309	67	1712	51	290
W		63	58	57	30	16	150	27	1
Zn		86	54	53	113	8	598	51	46
Zr		807	800	–	333	133	1444	51	380
Y		220	154	99	268	40	1827	51	n.g.
Ce		408	369	264	310	60	1874	51	n.g.
La		181	177	198	129	7	647	51	31
Nd		194	168	170	144	17	852	51	n.g.
Pr		32	31	34	24	1	129	51	n.g.
Sm		26	23	17	16	6	80	51	n.g.
Y+*REE*		1062	930	–	649	206	3009	51	
Zr/Hf		47.5							14.1
Th/U		17.2							5.0

S.D. = standard deviation; *n* = number of analyses; AB = average composition of bauxite (after Bronevoy *et al*., 1985); n.g. = not given

(BSEI) of a 'leucoxene' crystal (Fig. 2*a*), bright areas are enriched in Nb. Its distribution can be interpreted to result from a few centres of crystallization being united during growth into a relatively large grain. The W content, recorded by microprobe, is not high, but its distribution is also zonal. Figure 2*b,c* shows a W-rich core in a 'leucoxene' grain. It seems to be characteristic that very often the zoning observed does not follow any crystallographic direction (Fig. 3). The distribution of Fe and Nb is similar and the substitution $2Ti^{4+} \rightleftharpoons Fe^{3+}+Nb^{5+}$ seems very likely. The presence of V was also detected in fine 'leucoxene' grains (<5 μm) by X-ray mapping.

Since Ti oxides are absent in the parent rock, their formation as a result of weathering cannot be in doubt. The main source of Ti was ilmenite, as well as Ti-bearing minerals such as aegirine and riebeckite. Columbite might be the source of Nb,

TABLE 2. Correlation matrix of chemical element contents in the bauxite profile (36 samples).

	SiO_2	Al_2O_3	TiO_2	P_2O_5	Ba	Bi	Ce	Cr	Ga	Hf	La	Nb	Nd	Ni	Pb	Pr	Sc	Sm	Sr	Th	U	V	Y	Zn	Zr
SiO_2	1																								
Al_2O_3	−0.77	1																							
TiO_2	−0.03	0.02	1																						
P_2O_5	0.59	−0.56	−0.40	1																					
Ba	0.71	−0.64	−0.17	0.91	1																				
Bi	0.71	−0.75	−0.09	0.81	0.91	1																			
Ce	0.00	0.04	−0.18	0.30	0.20	0.18	1																		
Cr	0.31	−0.30	0.23	0.28	0.26	0.40	0.66	1																	
Ga	−0.30	0.21	−0.02	−0.14	−0.17	−0.14	0.48	0.21	1																
Hf	0.04	−0.13	0.89	−0.29	−0.06	0.09	0.03	0.37	0.11	1															
La	−0.07	0.06	−0.04	0.19	0.15	0.07	0.61	0.14	0.46	0.17	1														
Nb	0.10	−0.06	0.61	−0.40	−0.21	−0.08	0.19	0.38	0.01	0.75	0.19	1													
Nd	0.05	−0.06	−0.06	0.29	0.28	0.23	0.63	0.23	0.42	0.15	0.92	0.18	1												
Ni	0.74	−0.80	−0.30	0.73	0.75	0.72	−0.06	0.14	−0.25	−0.26	−0.10	−0.30	0.02	1											
Pb	0.50	−0.51	−0.09	0.65	0.73	0.78	0.65	0.62	0.23	0.21	0.39	0.19	0.48	0.44	1										
Pr	−0.07	0.06	0.01	0.15	0.12	0.06	0.59	0.16	0.45	0.22	0.99	0.25	0.93	−0.12	0.36	1									
Sc	−0.16	0.10	−0.17	0.19	0.15	0.12	0.62	0.35	0.49	0.07	0.45	0.20	0.42	−0.11	0.54	0.43	1								
Sm	0.04	−0.04	−0.19	0.39	0.33	0.27	0.89	0.46	0.49	0.04	0.84	0.12	0.90	0.03	0.65	0.81	0.57	1							
Sr	0.61	−0.62	−0.35	0.95	0.89	0.80	0.14	0.16	−0.21	−0.30	0.09	−0.45	0.15	0.82	0.55	0.05	0.08	0.23	1						
Th	0.16	0.05	0.07	−0.15	−0.05	−0.13	0.32	0.27	0.05	0.10	0.22	0.44	0.21	−0.08	0.18	0.22	0.23	0.25	−0.22	1					
U	0.16	−0.07	−0.17	0.45	0.29	0.28	0.54	0.44	0.35	−0.06	0.46	−0.15	0.48	0.19	0.45	0.44	0.32	0.59	0.31	0.07	1				
V	0.71	−0.71	−0.14	0.87	0.88	0.88	−0.04	0.26	−0.30	−0.08	−0.11	−0.28	−0.01	0.82	0.56	−0.13	−0.04	0.03	0.90	−0.21	0.29	1			
Y	0.01	0.01	−0.33	0.45	0.38	0.20	0.48	−0.05	0.27	−0.21	0.61	−0.29	0.62	0.17	0.36	0.53	0.29	0.68	0.33	0.13	0.44	0.13	1		
Zn	0.01	−0.10	−0.55	0.39	0.25	0.08	−0.26	−0.39	−0.19	−0.71	−0.19	−0.62	−0.16	0.49	−0.16	−0.22	0.05	−0.17	0.49	−0.17	−0.10	0.33	0.10	1	
Zr	0.17	−0.30	0.82	−0.05	0.16	0.30	0.05	0.40	0.06	0.96	0.19	0.63	0.17	−0.05	0.34	0.22	0.08	0.09	−0.05	−0.06	0.02	0.16	−0.13	−0.61	1

TABLE 3. Microprobe analyses (wt.%) of 'leucoxene' from bauxite profile.

	#2	#3	#12	#13	#15	#16	#18	#22	#23		
Na_2O	0.06	0.03	0.01	0.03	bdl	bdl	bdl	0.02	0.01	–	–
MgO	bdl	0.02	bdl	bdl	0.02	bdl	bdl	bdl	bdl	–	–
Al_2O_3	0.03	0.05	0.03	0.08	0.05	0.05	0.03	0.09	0.08	3.80	4.51
SiO_2	0.02	bdl	0.01	0.01	0.01	bdl	bdl	bdl	0.02	0.38	0.39
P_2O_5	0.08	bdl	bdl	bdl	0.01	0.04	0.04	0.02	bdl	–	–
K_2O	0.08	0.03	0.03	0.01	bdl	0.02	0.01	0.01	0.06	–	–
CaO	0.06	0.04	0.09	0.11	0.07	0.06	0.06	0.06	0.04	0.16	0.17
TiO_2	82.28	83.24	84.06	95.58	75.76	74.10	84.27	68.24	77.88	82.21	81.96
Fe_2O_3	3.69	4.20	3.94	0.32	6.86	7.52	3.95	9.15	6.19	0.73	0.80
MnO	bdl	bdl	bdl	bdl	bdl	bdl	bdl	bdl	bdl	–	–
SrO	0.02	0.02	bdl	0.02	0.03	bdl	bdl	bdl	bdl	–	–
Y_2O_3	0.04	0.04	0.06	bdl	0.02	bdl	bdl	bdl	0.04	–	–
ZrO_2	bdl	bdl	bdl	0.07	bdl	0.21	0.09	0.12	0.07	–	–
Nb_2O_5	10.50	9.19	9.54	0.43	14.83	16.06	8.99	19.77	12.28	–	–
BaO	0.72	0.71	0.67	0.68	0.64	0.68	0.74	0.58	0.77	–	–
La_2O_3	bdl	bdl	bdl	bdl	bdl	bdl	0.04	bdl	bdl	–	–
Ce_2O_3	0.34	0.24	0.33	0.41	0.29	0.36	0.33	0.18	0.27	–	–
Pr_2O_3	bdl	bdl	bdl	bdl	bdl	bdl	bdl	bdl	bdl	–	–
$-_2O_3$	bdl	bdl	bdl	bdl	bdl	bdl	bdl	bdl	bdl	–	–
Sm_2O_3	bdl	bdl	bdl	bdl	bdl	bdl	bdl	bdl	0.01	–	–
HfO_2	0.05	bdl	0.16	0.07	0.10	0.03	bdl	bdl	0.12	–	–
Ta_2O_5	bdl	0.04	0.10	bdl	bdl	bdl	0.01	0.13	bdl	–	–
PbO	0.05	0.06	0.10	bdl	0.07	0.06	bdl	0.14	bdl	–	–
ThO_2	bdl	bdl	bdl	bdl	bdl	bdl	bdl	bdl	bdl	–	–
UO_2	0.07	bdl	0.16	bdl	bdl	bdl	0.06	0.01	bdl	–	–
F	0.04	bdl	bdl	0.05	bdl	bdl	0.04	bdl	bdl	–	–
Cr_2O_3	–	–	–	–	–	–	–	–	–	1.19	1.27
WO_3	–	–	–	–	–	–	–	–	–	1.08	1.35
Total	98.13	97.91	99.29	97.87	98.76	99.19	98.66	98.50	97.82	89.55	90.45

bdl: below detection limit; –: not determined.

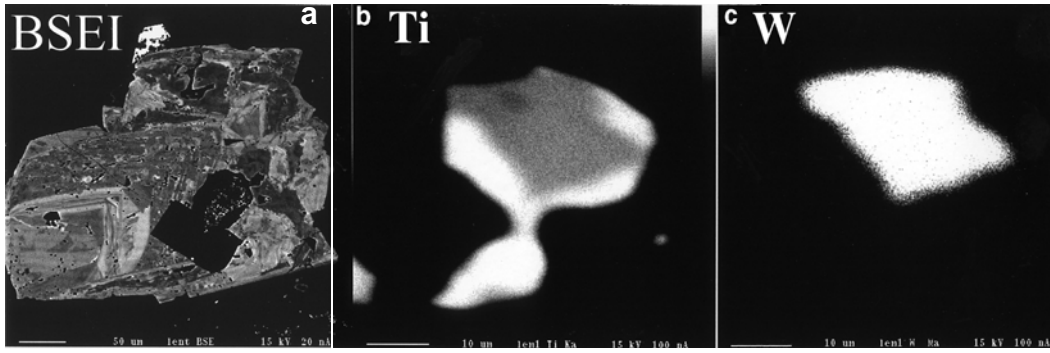

FIG. 2. 'Leucoxene' from bauxite: (*a*) Back Scattered Electron Image (BSEI) of a 'leucoxene' grain (bar = 50 μm). Bright areas correspond to increased Nb content; X-ray maps of distribution of Ti (*b*) and W (*c*) in 'leucoxene'.

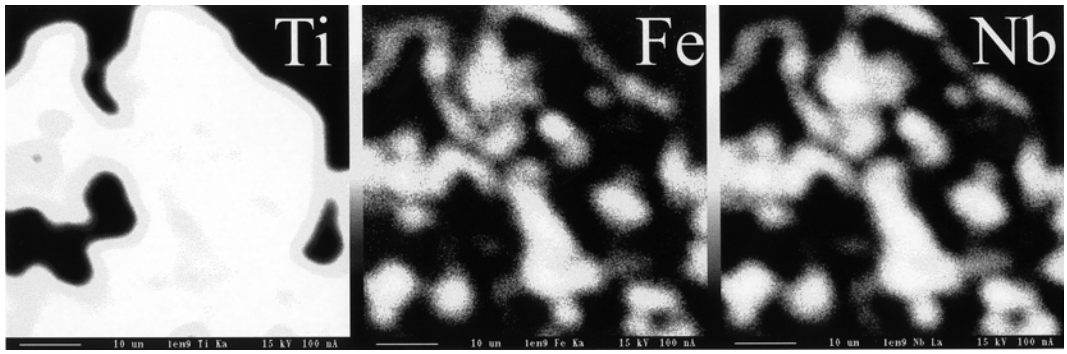

FIG. 3. X-ray maps of elemental distribution in 'leucoxene'. The distribution of Fe and Nb is similar.

as its remains are strongly leached within the profile. The origin of W and Cr is not so clear, as they have not been traced in the source rock. One occurrence of Zn chromite was recorded in bauxite. 'Leucoxene' seems to be the main concentrator of Cr and W and a very important concentrator of Nb within the profile. Frequently, zircon crystals of 1–2 μm in size serve as crystallization centres for 'leucoxene'. The veined character of Ti distribution and its spatial association with crandallite group minerals (Fig. 4) obviously point to some Ti mobility during bauxite formation.

In the late stages of profile development, 'leucoxene' was also the subject of alteration as well. Figure 5 illustrates leaching of a 'leucoxene' grain with precipitation of boehmite in a leached hole. This could be related to the process of hydrothermal alteration of a primary profile (Mordberg, 1997).

Crandallite group minerals

Crandallite group minerals are very common in both karst and laterite bauxite environments. According to Gaines *et al*. (1997), the general formula of 'crandallite' is $AB_3(TO_4)_2(OH)_5H_2O$, where A = Ca, Sr, Ba, Pb; B = Al, Fe^{3+}; and T = As, P. Also distinguished is a florencite group $AB_3(TO_4)_2(OH)_{5\text{ or }6}$ with A = *REE*, Bi, Ca, Th, Pb, □; B and T are the same, and beudantite group $AB_3(XO_4)_2(OH)_6$ where A = Ba, Ca, Pb, Sr; B = Al, Fe^{3+}; X = S, As, P. Uniting these formulae and taking into account possible solid solutions, we can write the general formula for the natural minerals belonging to all three groups as

$$AB_3(XO_4)_2(OH)_5H_{0-1}(OH)_{0-1}$$

where A = Ca, Ba, Sr, Pb, Bi, *REE*, Th, □; B = Al, Fe^{3+}; and X = P, As, S. The number of H and OH depends on cation charge in the A position and anion charge in the X position.

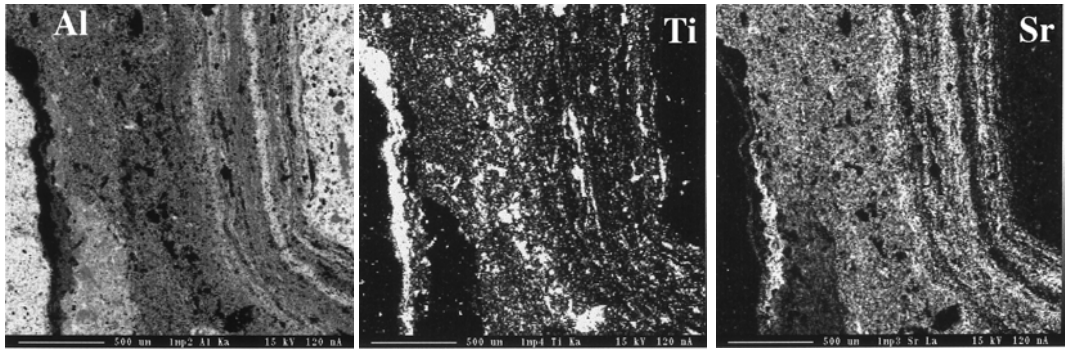

FIG. 4. X-ray maps of Ti, Al and Sr distribution in bauxite. Sr represents crandallite mineralization.

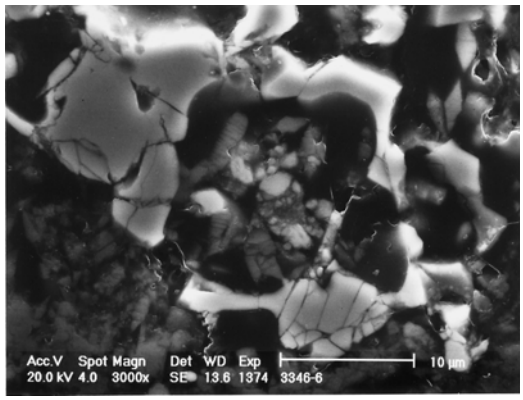

FIG. 5. Boehmite crystals in a hole leached in 'leucoxene' (SE image).

Crandallite itself, $CaAl_3(PO_4)_2(OH)_5H_2O$, has been recorded in karst bauxite deposits of Hungary, Pacific islands (Bárdossy, 1982) and Jamaica (Anderson, 1971). It is also the principal mineral of lateritic profiles over P-rich rocks in the Eastern Amazon Region where it was found in association with other aluminous phosphates such as augelite, variscite, wavellite, etc. (Schwab *et al*., 1983). Bushinsky (1975) noted a typical association of P, Sr and S in bauxite profiles. Svanbergite $SrAl_3(PO_4)(SO_4)(OH)_6$ has been recorded in the Tikhvinsk deposit (Ansheles and Vlodavets, 1927), in the few occurrences of the N Urals (Lukanina, 1959; Beneslavsky, 1974), among bauxitic clays of Portugal (Gomes, 1968) and in lateritic bauxite profiles of the Kursk Magnetic Anomaly (Bulgakova, 1967; Makarov, 1967). It is an essential mineral of the Zaostrovsk bauxite-phosphorite occurrence (Mordberg, 1999). A mineral with a composition intermediate between Nd-florencite, goyazite and crandallite occurs in the bauxite deposit of Vlasenica, Yugoslavia (Maksimović and Panto, 1985). Gorceixite and florencite were recorded in the Lohrheim kaolinitic deposit, Germany (Dill *et al*., 1995). Minerals of the crandallite group, such as goyazite, gorceixite and florencite, have been observed in bauxitic kaolins of NE Sudan (Wipki, 1995; Germann *et al*., 1995; Schwarz and Germann, 1999). Within the studied deposit, crandallite was recorded by Likhachev (1993). It is absent from the parent rock.

X-ray maps of element distribution (Fig. 6) show the following characteristics of crandallite group minerals. Although the size of the crystals is rather small (no more than 20–30 μm, usually 1–5 μm), the elements show a very clear zonal distribution. The sequence of element accumulation within a crystal from its core to its rim is: Ca → Ba, Ce, S → Ca → Pb, Ce → Sr, S. Thus, at least three elements (Ca, Ce and S) show more than one zone of accumulation. Iron shows an irregular distribution in the internal part of the crystal which seems to be typical of this element. Accumulation in the rim is characteristic of *REE* and Pb. This zonal distribution of elements can be seen even from very small grains around a relatively big crystal (Fig. 6). From the selected microprobe analyses (Table 4), it can be seen that none of the analysed points belongs to one or other end-member. However, from the chemical composition, varieties are distinguished, such as Sr-rich woodhouseite and/or svanbergite, Ca-rich crandallite, Pb-rich plumbogummite and/or hinsdallite, and *REE*-enriched florencite. It seems that pure end-members may exist within very thin zones which can be traced on X-ray maps, but the beam spot size does not permit single point analysis.

Calculation of the 'crandallite' formula from microprobe analyses based on 14 oxygen atoms shows a constant lack of anions (P and S), while the number of Al ions is always >3. The average of 27 microprobe analyses is shown in the formula

$$A_{1.03\pm0.01}B_{3.41\pm0.05}(XO_4)_{1.89\pm0.03}$$

(determined at 95% confidence interval) which obviously does not fit the stoichiometry of crandallites. Correlation analysis of bulk geochemical data (Table 2) shows a very high positive correlation of Sr and Ba with both Bi and V. The correlation of the last two elements with Pb and P is also positive. No other correlation was found for Bi and V. This suggests the incorporation of both V and Bi into the crandallite lattice. Although the substitution of V for P in crandallites has not been described in recent reviews (Gaines *et al*., 1997), it is well known for apatite (Nathan, 1984). Recalculation of the formula of crandallite assuming the number of Al atoms to be =3 and the presence of Fe^{2+} gives

$$A_{1.04\pm0.04}B_3(XO_4)_{1.73\pm0.06}$$

with a lack of anions and more than enough *A* cations. The assumption that Al+ Fe^{3+} = 3 gives

$$A_{0.91\pm0.02}B_3(XO_4)_{1.67\pm0.05}$$

Thus, none of the calculations gives the correct formula. All of them show a lack of anions, so

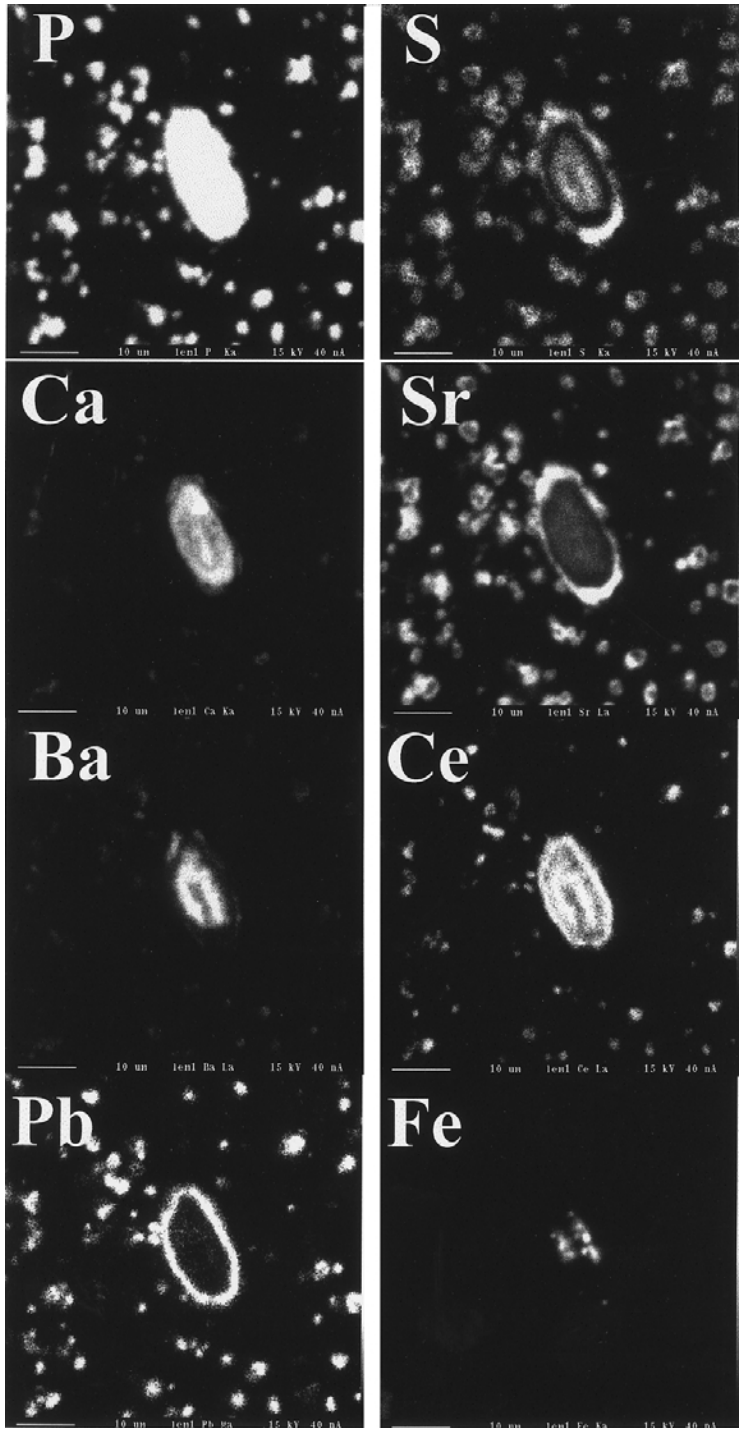

FIG. 6. X-ray maps of elemental distribution in 'crandallite' crystal and surrounding finely dispersed crandallite mineralization.

TABLE 4. Selected microprobe analyses of crandallite group minerals (wt.%).

	#7	#63	#21	#19	#20	#23	#18	C1	C2
Al_2O_3	34.00	36.24	33.98	34.72	37.00	34.06	31.97	30.64	22.26
P_2O_5	32.63	29.01	27.73	25.81	24.11	23.22	27.11	19.21	15.98
SO_3	1.08	1.92	0.71	0.68	0.66	2.69	0.96	1.64	1.10
Y_2O_3	0.49	0.77	1.83	2.41	1.50	0.88	1.18	nd	nd
SrO	2.30	5.88	2.21	1.89	1.18	4.00	2.81	2.85	2.25
CaO	8.39	6.22	4.98	2.74	2.23	4.27	6.01	1.49	0.92
Fe_2O_3	1.21	0.74	2.45	0.90	0.85	0.73	7.77	1.75	17.22
Ga_2O_3	bdl	bdl	0.12	0.03	bdl	bdl	0.01	nd	nd
BaO	2.91	2.22	5.05	2.73	1.35	1.85	4.64	nd	nd
La_2O_3	0.35	0.52	0.60	0.31	1.07	0.70	0.94	0.65	0.84
Ce_2O_3	0.39	0.90	bdl	0.51	2.18	1.87	0.08	5.88	4.63
Pr_2O_3	bdl	bdl	bdl	0.07	0.69	0.02	bdl	nd	nd
Nd_2O_3	1.49	0.60	1.60	4.85	6.68	2.12	1.03	nd	nd
Sm_2O_3	0.79	0.19	1.36	3.52	5.70	0.91	0.91	nd	nd
Gd_2O_3	0.61	0.22	1.56	3.52	3.47	0.76	0.96	nd	nd
Dy_2O_3	0.26	0.23	0.71	1.30	1.32	0.42	0.42	nd	nd
Er_2O_3	0.01	0.24	0.18	0.28	0.08	0.17	0.08	nd	nd
Yb_2O_3	0.06	0.11	0.14	0.05	0.09	0.09	bdl	nd	nd
PbO	0.66	2.22	1.45	1.59	2.19	8.43	1.35	15.78	13.44
Total	87.63	88.23	86.68	87.89	92.33	87.20	88.21	79.89	78.64
$Y+REE_2O_3$	4.37	3.43	7.66	16.48	22.60	7.68	5.52		

bdl: below detection limit

that the presence of V seems very likely. Another problem is the valence of Fe. Within the known species, it appears only as Fe^{3+} in the *B* position. However, from the calculations above, we may assume either the presence of both Fe^{3+} and Fe^{2+} or a certain amount of substitution of Bi for Ca and *REE* with formation of waylandite compound. Seven additional microprobe analyses of 'crandallite' determined 0.15−0.41 wt.% Bi and 0.04−0.07 wt.% V.

The formation of crandallite group minerals took place during weathering. Such a complicated composition of 'crandallite' crystals can be related to the rates of dissolution of minerals from the parent rock, the source of P being primary apatite. Two methods of crandallite formation are described: a direct replacement of apatite by attack of the weathering solution (Viellard *et al*., 1979) and the formation via apatite dissolution and following precipitation (Schwab *et al*., 1989). Both partial dissolution and direct alteration could have taken place. This explains the Ca-enriched core and Pb-, Sr- and *REE*-rich rims: the source of Pb and S was primary galena and pyrite, and the source of the *REE* could be bastnaesite in the parent rock which is more resistant to weathering.

Zircon and xenotime

In the parent rock, zircon and xenotime occur in the form of very small rare crystals usually <5 μm across, and do not contain any admixture. Within the bauxite profile, both minerals show clear traces of alteration or even growth during weathering. Their relationship can be understood better from Fig. 7 which represents the inherited remains of zircon and xenotime cemented by a solid solution of zircon and xenotime. Six microprobe analyses of this aggregate (Table 5) show that some elements such as Sc, Ca and Al are highly concentrated in this solid solution. It was assumed by Mordberg and Spratt (1998) that rather small mineral inclusions might occur within altered or neoformed areas of zircons. Figure 8 illustrates the appearance of a zircon crystal with these inclusions which cannot be identified precisely due to their small size (<500 nm). The low analytical total suggests that the altered zircon is metamict, and with essential H_2O rather than adsorbed H_2O in

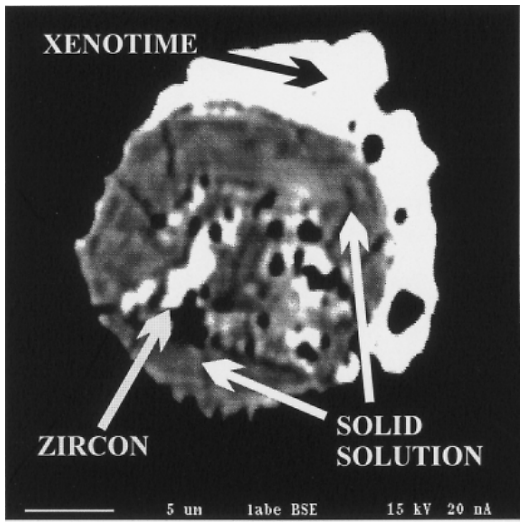

FIG. 7. Weathered remains of xenotime and zircon cemented by metamict solid solution of xenotime and zircon (BSEI). Analyses are given in Table 4.

radiation-induced defects since it is almost U-free, and the Th content does not exceed a few per cent. The Zr/Hf ratio in metamict zircon (37.1) is slightly lower than that in pure zircon (39.9), and suggests a certain fractionation of these elements during weathering due to the higher mobility of Zr. However, both zircons have lower Zr/Hf than the bulk (Table 1).

Zircon is a mineral which commonly occurs in very small amounts in several lateritic deposits where it is inherited from the parent rock (Bárdossy and Aleva, 1990). It has also been identified in many karstic deposits (Bárdossy, 1982). Sometimes, detailed investigations fail to detect zircon within bauxite profiles even though the Zr content may be high (Melfi *et al*., 1996). Nevertheless, Zr has been used many times for the purpose of identification of source material assuming its immobility during weathering. The presence of small amounts of Y, P and Sc has been identified in zircon from the bauxite deposits at Mazaugues (France) and Campo Felice (Italy). However, zircon was regarded as a detrital mineral, with Y and Sc considered to substitute for Zr (Bárdossy and Panto, 1973).

Monazite

Monazite seems to be the least altered mineral of the bauxite profile. Only slight alteration of monazite grains with some incorporation of Al along cracks was observed. Typically, within the profile 10–20 small monazite grains occur close to each other, so that they look like a physically destroyed larger crystal. Monazite from the bauxite profile usually contains some Si, Ca and Th (Table 6). It was suggested that monazite can form during lateritic weathering of *REE*-bearing baryte and apatite from a profile over carbonatites in Siberia (Slukin *et al*., 1989).

Pyrochlore and columbite

Pyrochlore and columbite were recorded in both the parent rock and weathering profile. Usually, the size of crystals does not exceed

TABLE 5. Microprobe analyses (wt.%) of xenotime (1), zircon (6) and metamict zircon (2–5) from Fig. 7.

	1	2	3	4	5	6
Na_2O	0.02	0.03	0.02	0.06	0.05	0.02
Al_2O_3	0.19	1.17	0.78	1.33	0.99	0.15
SiO_2	0.28	24.51	25.28	21.95	22.69	31.02
ZrO_2	bdl	55.80	54.02	51.24	50.94	65.05
P_2O_5	28.44	1.19	3.20	2.79	3.76	0.33
CaO	0.12	1.26	0.63	1.45	1.23	0.16
Sc_2O_3	0.08	1.97	1.52	3.33	2.35	0.32
Y_2O_3	37.02	3.50	4.21	4.44	5.77	0.51
HfO_2	bdl	1.71	1.29	1.48	1.31	1.30
Total	66.14	91.16	90.94	88.06	89.07	98.86

bdl: below detection limit

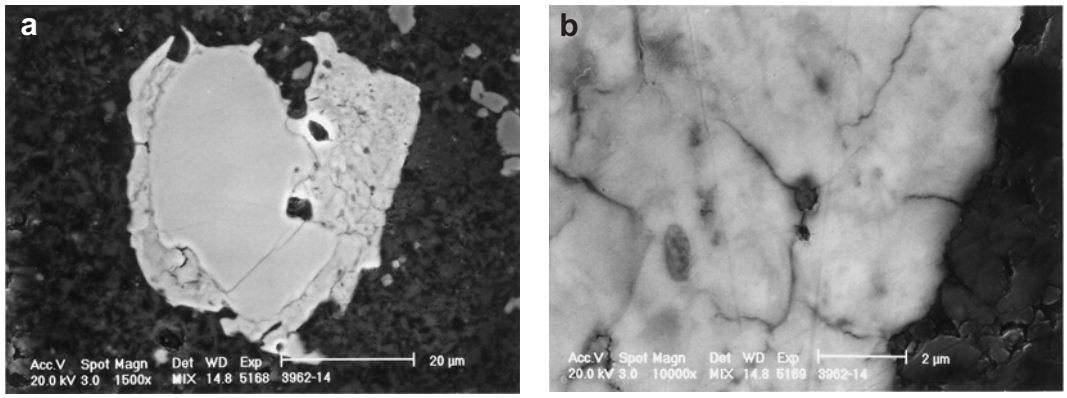

FIG. 8. Alteration of zircon: (*a*) a crystal of stoichiometric zircon inherited from the parent rock surrounded by metamict zircon; (*b*) closer view of metamict zircon showing the presence of inclusions.

50 µm. Both minerals seem much less abundant in the profile than Nb-bearing 'leucoxene' which indicates that the latter is the main concentrator of Nb. Columbite is strongly leached within the profile, and is sometimes intergrown with 'leucoxene'. X-ray maps of elemental distribution (Fig. 9) show that Pb is enriched mainly in the rims of pyrochlore crystals, while the core is relatively enriched in Ca. The distribution of Na is also zonal. The PbO content varies from 5 wt.% in the core of a crystal to 16 wt.% in the rim (Table 7); other elements found in pyrochlore are Sr (1−2%), Ba (0.3−0.9%), Ce (up to 0.9%), Th (0.4−1.9%) and Ti (1.1−1.9%). An analysis of the core corresponds to the formula $A_{1.89}B_{2.06}O_6$(O,OH,F), and the average formula of five analyses of the rim is $A_{1.74}B_{2.11}O_6$(O,OH,F), where B = Nb, Ta and Ti, and the other elements are A site cations. The formula coefficient of Ca decreases from 0.87 in the core to 0.79 in the rim, while the coefficients of other elements increase (from 0.09 to 0.24 for Pb, from 0.24 to 0.53 for Na, etc.).

Slukin *et al*. (1989) showed clearly the alteration and growth of pyrochlore during lateritization of carbonatites in Siberia with the formation of Sr-, Ba- and *REE*-rich rims around Ca-pyrochlore. Wall *et al*. (1996) demonstrated that the initial weathering of pyrochlore may be expressed in leaching and partial exchange of A cations which lead to their dramatic depletion. They also observed local concentrations of Sr-, Ba- and Ca-rich pyrochlore poor in Na, and a number of Ce- and K-pyrochlore rims. The present case seems to be quite similar to those described. The difference is the presence of Pb in the rims. In the pyrochlore from the parent rock, the PbO content is not greater than 2.5 wt.% (Likhachev, 1993). Wall *et al*. (1996) also found an intergrowth of pyrochlore and crandallite in the most weathered part of the profile over carbonatites at Lueshe, Zaïre. Although a similar intergrowth was not observed in the studied profile, an association between these two minerals exists, as can be seen from the Ca distribution (Fig. 9): rather small points around the crystal represent crandallite mineralization.

Th-Zr-Y mineralization

An unidentified mineral from the parent rock was analysed (Table 8). This is a Th- and Fe-rich phosphate-silicate which also carries significant Ca and Y. Assuming the number of oxygen atoms is 5, the average formula of the mineral was calculated as

$$(Fe^{2+}_{0.81}Ca_{0.14}Na_{0.05})_{\Sigma=1.00}(Th_{0.85}Y_{0.08}REE_{0.04}U_{0.01})_{\Sigma=0.99}(Si_{0.81}P_{0.16}S_{0.02}O_4)(OH_{0.89},F_{0.11})_2$$

which can be simplified as

$$Fe^{2+}Th(Si,PO_4)(OH,F)_2$$

A strongly weathered Th-rich mineral occurs within the weathering profile, it differs from the parent rock mineral in having a decreased Th content and by containing essential Zr (Table 9). The mineral demonstrates clear traces of radioactive decay and may be partially decomposed (Fig. 10*a*). It is of interest that an intergrowth of galena and pyrite sometimes occurs next to the

TABLE 6. Average chemical composition (wt.%) of monazite from bauxite (14 microprobe analyses).

	SiO_2	P_2O_5	CaO	Y_2O_3	La_2O_3	Ce_2O_3	Pr_2O_3	Nd_2O_3	Sm_2O_3	Gd_2O_3	PbO	ThO_2	UO_2	Total
Mean	0.49	27.42	0.48	0.12	15.33	29.30	4.89	13.08	2.68	3.45	0.02	2.37	0.03	99.66
Standard error	0.08	0.10	0.07	0.04	1.17	0.80	0.08	0.86	0.41	0.14	0.01	0.45	0.00	0.15
Median	0.42	27.47	0.46	0.03	14.59	29.54	4.92	13.34	2.38	3.47	0.00	1.87	0.03	99.70
S.D.	0.29	0.39	0.26	0.14	4.39	3.01	0.29	3.23	1.55	0.53	0.05	1.67	0.01	0.56
Min	0.22	26.58	0.18	0.00	10.45	22.98	4.22	5.90	0.50	2.50	0.00	0.82	0.01	98.98
Max	1.20	28.14	1.06	0.33	26.47	33.28	5.23	17.71	4.89	4.20	0.18	7.18	0.05	100.67

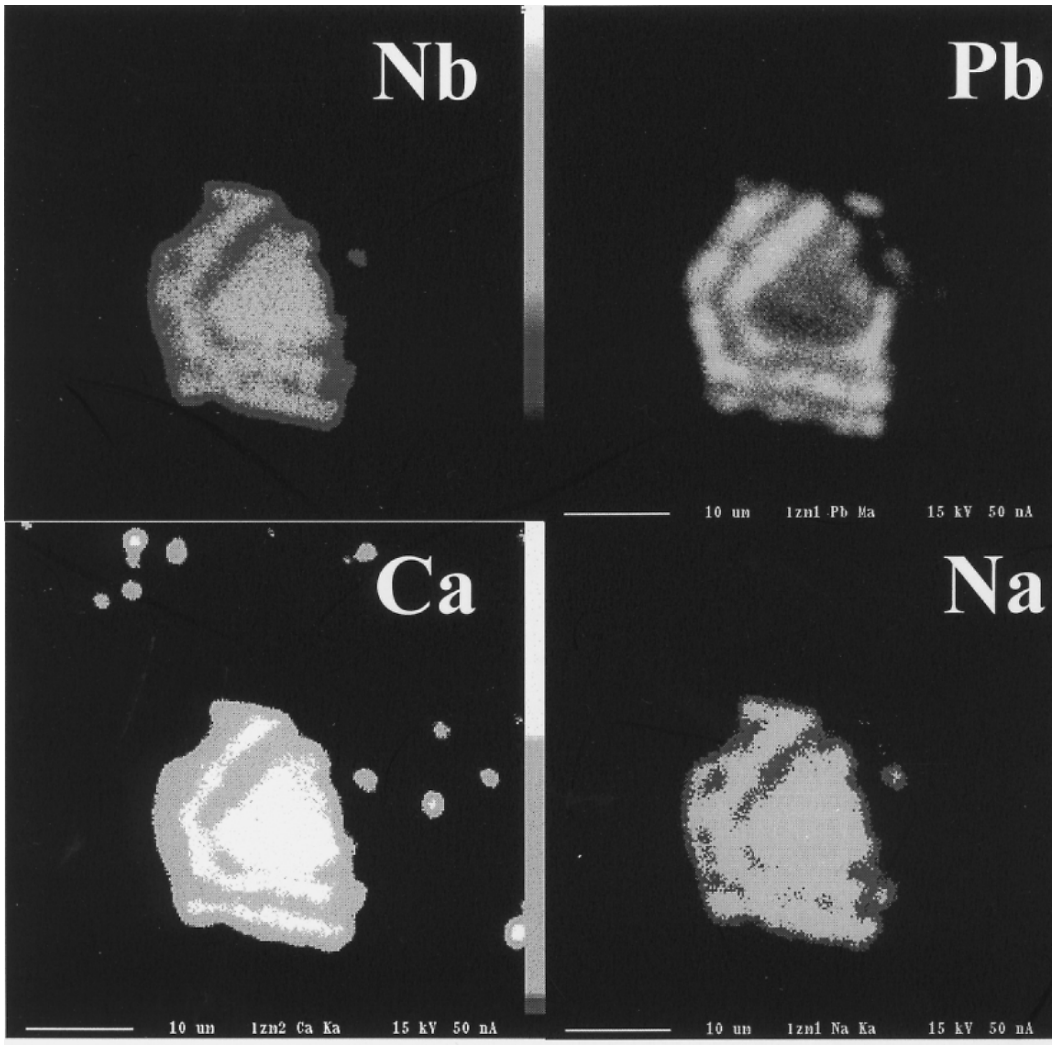

FIG. 9. X-ray maps of elemental distribution in pyrochlore.

TABLE 7. Microprobe analyses of pyrochlore from the bauxite profile (wt.%).

	#4	#5	#6	#10	#11	#14
Na_2O	3.98	4.17	6.49	3.06	2.82	4.51
MgO	0.01	bdl	bdl	0.02	bdl	0.02
Al_2O_3	0.02	0.02	0.01	0.35	0.09	0.27
K_2O	0.03	bdl	0.10	0.26	0.11	0.01
CaO	10.66	10.67	12.56	10.20	10.03	8.68
MnO	bdl	0.01	bdl	bdl	bdl	0.01
FeO	0.39	0.34	0.40	0.54	0.27	0.82
SrO	2.40	1.80	1.12	1.33	1.60	1.87
Y_2O_3	0.02	0.08	0.04	bdl	0.02	bdl
BaO	0.90	0.71	0.32	0.38	0.44	0.04
La_2O_3	0.23	0.24	0.25	0.08	0.17	0.01
Ce_2O_3	0.86	0.92	0.65	0.34	0.56	bdl
Pr_2O_3	bdl	0.10	bdl	bdl	bdl	bdl
Nd_2O_3	0.13	0.14	0.14	0.06	0.21	bdl
Sm_2O_3	bdl	bdl	bdl	bdl	bdl	bdl
PbO	9.27	10.61	5.17	12.05	16.01	11.83
ThO_2	0.47	0.53	0.74	0.41	0.55	1.92
UO_2	bdl	bdl	0.20	0.14	0.06	0.19
TiO_2	1.45	1.64	1.89	1.31	1.09	1.41
Nb_2O_5	64.99	65.16	67.49	56.46	62.88	56.42
Ta_2O_5	0.13	bdl	0.20	0.04	0.57	bdl
ZrO_2	0.09	0.01	bdl	bdl	bdl	0.02
HfO_2	bdl	0.14	0.20	bdl	0.11	0.17
SiO_2	bdl	bdl	bdl	0.30	bdl	bdl
P_2O_5	bdl	bdl	bdl	bdl	bdl	bdl
F	1.45	1.40	2.16	0.98	0.85	1.44
Total	97.47	98.66	100.10	88.29	98.41	89.64

bdl: below detection limit

mineral grains (Fig. 10*b*). From X-ray maps of the element distribution (Fig. 11), the shape of the original crystal can be identified. Some redistribution of elements such as Ca and P is also seen. It is clear from microprobe analyses of the mineral (Table 9), that the contents of P, Ca, Y, Zr and especially of Fe vary within the analysed grains. Twelve microprobe analyses of *REE* (Ce, La, Pr, Nd, Sm and Gd) in the mineral from bauxite show that only two are present in amounts greater than the detection limit: the Ce content varies from 800 to 1500 ppm, and the Gd content is 0.12−0.43%. Elements such as Ti, W and U are always present in amounts <1%. None of the analogous minerals was found by the authors in the literature or in any modern database. The attempts at formula calculation were made using analyses from the central, less altered parts of crystals. The most appropriate results were obtained assuming that the number of oxygen atoms is 14 and the low total derived from the presence of water:

$$(Fe^{2+}_{3.67}Ca_{0.28})_{\Sigma=3.95}(Zr_{1.31}Th_{0.91}Y_{0.41}Al_{0.42}Ti_{0.07})_{\Sigma=3.12}((Si_{1.32}P_{0.58})_{\Sigma=1.9}O_8)O_6\cdot 6H_2O$$

It can be generalized as $A_4B_3(XO)_2O_6\cdot 6H_2O$ where $A = Fe_{2+}$, Ca,; B = Zr, Th, Al; and X = Si, P, (S?). However, since the structure of the mineral is unknown, the correct formula is a subject for further study. The mineral seems to be metamict, and as its radioactivity is very high, we may assume the presence of adsorbed H_2O in radiation-induced defects.

The relationship between the two Th-bearing minerals is not quite clear. Two possibilities can be discussed: (1) there are two different minerals occurring in the parent rock and weathering

TABLE 8. Chemical composition (wt.%) of an unknown mineral from the parent rock (average of 18 microprobe analyses).

	Mean	Median	S.D.	Min	Max
Na_2O	0.41	0.43	0.11	0.18	0.58
MgO	0.05	0.05	0.02	0.02	0.09
Al_2O_3	0.17	0.15	0.05	0.10	0.30
SiO_2	12.00	11.91	1.07	10.00	13.77
P_2O_5	2.86	2.64	0.74	1.58	4.00
SO_3	0.39	0.38	0.16	0.15	0.93
K_2O	0.09	0.09	0.02	0.07	0.13
Y_2O_3	1.96	2.03	0.68	0.56	2.90
CaO	2.07	2.03	0.19	1.74	2.45
TiO_2	0.06	0.07	0.04	0.00	0.13
MnO	0.08	0.06	0.08	0.00	0.28
FeO	15.49	15.27	2.82	11.49	21.34
ZrO_2	0.08	0.00	0.19	0.00	0.63
La_2O_3	0.04	0.02	0.05	0.00	0.16
Ce_2O_3	0.37	0.32	0.17	0.13	0.69
Pr_2O_3	0.03	0.00	0.05	0.00	0.15
Nd_2O_3	0.34	0.31	0.21	0.04	0.71
Sm_2O_3	0.07	0.05	0.09	0.00	0.32
Gd_2O_3	0.33	0.34	0.16	0.03	0.60
Dy_2O_3	0.33	0.33	0.12	0.07	0.54
Er_2O_3	0.18	0.22	0.09	0.00	0.31
Yb_2O_3	0.08	0.06	0.08	0.00	0.24
HfO_2	0.04	0.00	0.10	0.00	0.28
WO_3	0.22	0.19	0.20	0.00	0.62
PbO	0.21	0.21	0.06	0.08	0.29
ThO_2	54.45	55.45	2.66	47.88	58.17
UO_2	0.74	0.76	0.11	0.56	0.94
F	1.00	1.06	0.24	0.15	1.17
Total	94.15	93.95	1.57	91.11	97.11

profile, and (2) the mineral from the weathering profile is a result of alteration of the mineral from the parent rock. The latter case seems more likely and can be related to hydrothermal alteration of a primary weathering profile (Mordberg, 1997). A Zr/Hf ratio of 48.1 is much higher than those from both pure and metamict zircons but is close to the ratio in the whole rock.

Galena and pyrite

Sulphide mineralization is known in the parent rock. It involves mainly pyrite, galena and sometimes sphalerite (Likhachev, 1993). During weathering under oxidizing conditions, sulphides disappear completely. Pseudomorphic replacement of pyrite with hematite is typical. Sometimes, such a pseudomorph can be surrounded by a zone of bleaching of a few cm diameter. The appearance of both pyrite and galena is related to two processes: the partial decomposition of the unnamed Th-rich mineral with the release of Fe and Pb (Fig. 10) and hydrothermal alteration of the weathering profile under reducing conditions. The latter process is expressed in almost total removal of Fe and the formation of muscovite veins which cross the original profile zoning (Mordberg, 1997). The observed intergrowths of pyrite and galena are also typical of this process (Figs 12, 13); sometimes pyrite forms a core and galena surrounds it (Fig. 13), at other times the reverse is the case (Fig. 12). This hydrothermal generation of sulphides bears chalcophile elements, some of which show a discrete distribution (Cu, Bi and Ni) while others (As, Ag and Cd) are distributed evenly (Figs 12, 13).

TABLE 9. Chemical composition (wt.%) of an unknown silicate-phosphate mineral from bauxite (average from 9 microprobe analyses).

	Mean	Median	S.D.	Min	Max
SiO_2	8.78	8.55	1.25	7.07	10.77
Al_2O_3	1.49	1.56	0.65	0.54	2.39
P_2O_5	5.43	4.93	1.36	4.09	7.63
CaO	1.98	2.00	0.42	1.52	2.58
TiO_2	0.75	0.67	0.41	0.20	1.48
FeO	20.46	22.89	9.57	3.59	30.17
Y_2O_3	6.72	5.96	2.14	4.36	9.98
ZrO_2	17.63	16.61	2.65	14.44	22.75
HfO_2	0.32	0.30	0.06	0.23	0.40
WO_3	0.44	0.44	0.19	0.21	0.79
PbO	0.20	0.11	0.31	0.01	1.02
ThO_2	24.85	23.91	2.33	22.13	29.47
UO_2	0.25	0.23	0.04	0.21	0.32
Total	89.29	88.94	1.83	86.09	92.50

Discussion

It can be seen from the above data, that almost all the accessory minerals from the parent rock have either disappeared (ilmenite, bastnaesite, galena, pyrite, etc.) or have been strongly altered (zircon, pyrochlore, xenotime, etc.) during bauxitic weathering. The appearance of some minerals such as 'leucoxene' and 'crandallite' is a direct result of weathering. Both altered and neoformed minerals show a clear zonal distribution of chemical elements, usually unrelated to crystallographic directions within a grain. This reflects the low-temperature slow process of their formation. Another characteristic feature of the composition of minerals formed during weathering is the presence of Al and Fe with random distribution within the crystals. This points to their high activity in weathering solutions.

The supposed scheme of mineral transformation during bauxite weathering is given in Fig. 14. Most of the trace elements tend to accumulate in

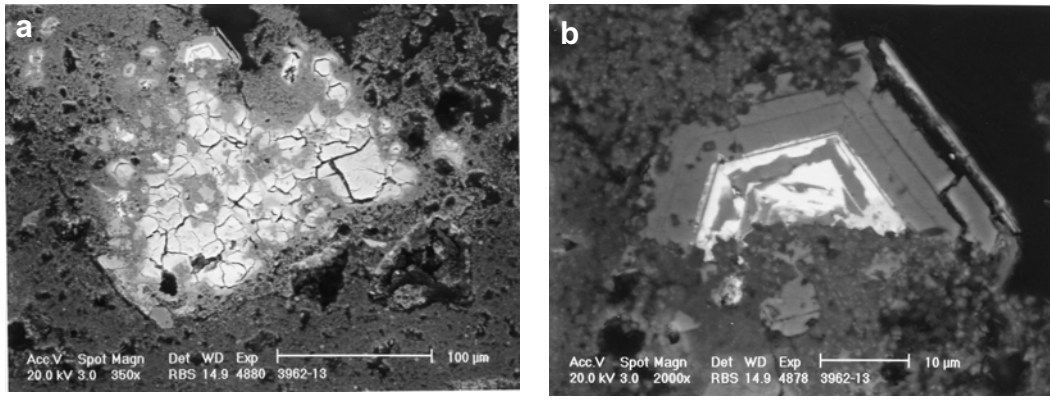

FIG. 10. (*a*) Partially decomposed Zr-Th-Y-bearing phosphosilicate from bauxite; (*b*) an intergrowth of galena (bright) and pyrite (grey). The crystal can be seen in the upper part of Fig. 10*a*.

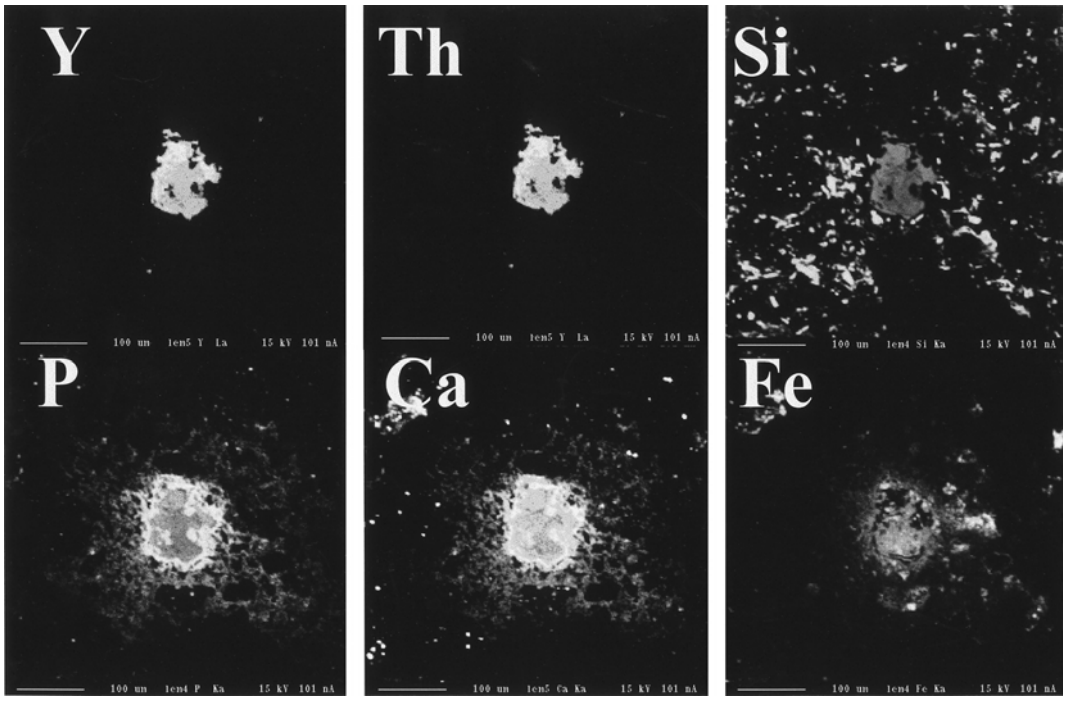

FIG. 11. X-ray maps of elemental distribution in Zr-Th-Y-bearing phosphosilicate from bauxite. Redistribution of P and Ca and partial removal of Fe are seen.

accessory minerals of bauxite. This process takes place through the dissolution of the majority of the initial minerals. Almost every element is distributed among a few mineral phases in the parent rock. For example, P occurs in monazite, xenotime and apatite. That held in monazite is almost immobile; however, P from apatite went into solution during weathering, providing acidic media. This part could be removed from the profile, but the presence of alkaline earths, Pb and *REE* with high activities of Al and Fe led to their joint precipitation in the form of crandallite group minerals. Sodium, known to be particularly mobile during weathering, shows much less mobility if it exists in the form of pyrochlore. Some mobility of known 'immobile' elements such as Ti, Cr and Nb is seen from the formation of Cr- and Nb-bearing 'leucoxene'. However, this mobility is usually restricted by the volume of the weathered sequence. The *REE* from monazite are relatively immobile. However, their presence in 'crandallite' which is obviously a mineral syngenetic to weathering, points to their great mobility which was restricted by P and S.

Indeed, all the mineralogical changes take place on a background of downward (Maksimović, 1976) or lateral (Valeton, 1972) movement of elements. The accummulation of base metals (Maksimović, 1976) or alkali elements (Mordberg *et al*., 1997) above the carbonate footwall seems to be quite important. The processes of sorbtion on or incorporation into Al- and Fe-oxides, oxyhydroxides and clay minerals seem to play a lesser role for the majority of trace elements if compared to the formation and alteration of accessory minerals.

Conclusions

The following conclusions can be drawn from the patterns described. This study shows that majority of trace elements tend to concentrate in the accessory minerals of bauxite, each element being distributed among a few of them. Only a few elements seem to associate with the rock-forming minerals, such as Ni in Fe-oxides or Ga and V in boehmite. Although the crystal size of the accessory minerals is rather small, the history of

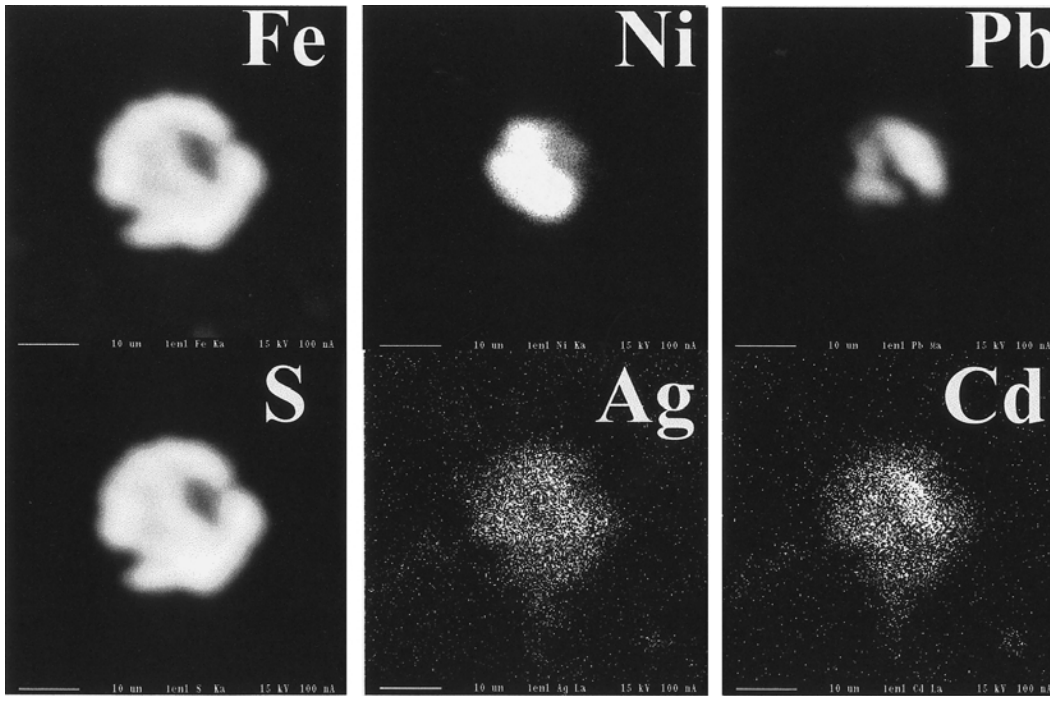

FIG. 12. X-ray maps of elemental distribution: an intergrowth of galena and pyrite. Galena forms the core.

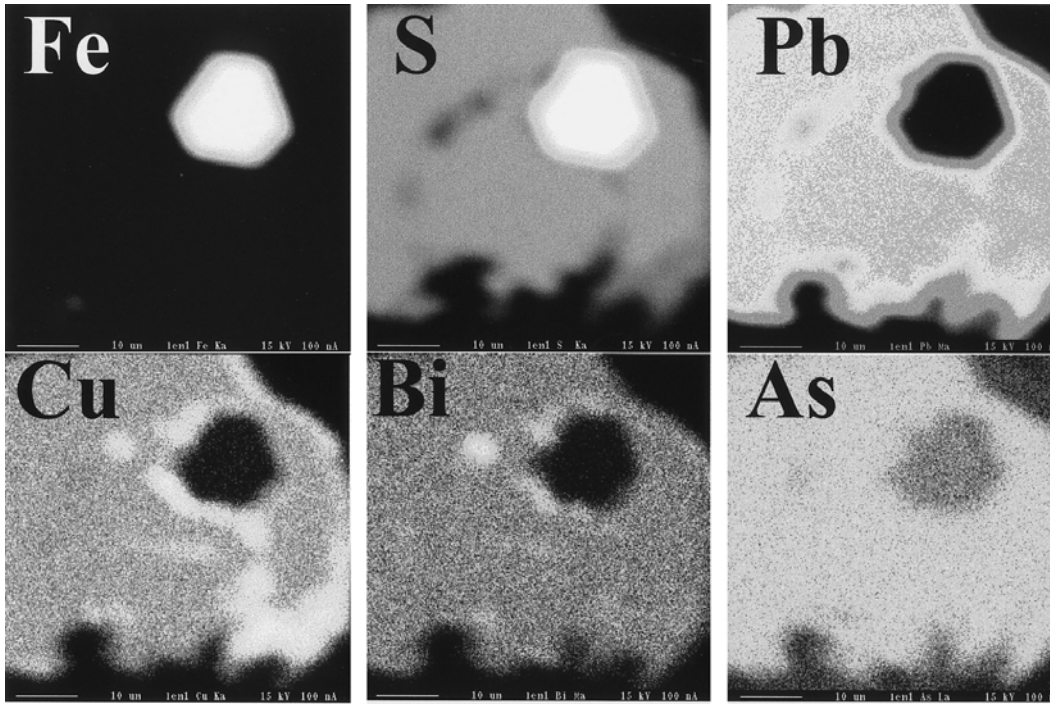

FIG. 13. X-ray maps of elemental distribution: an intergrowth of galena and pyrite. Pyrite forms the core.

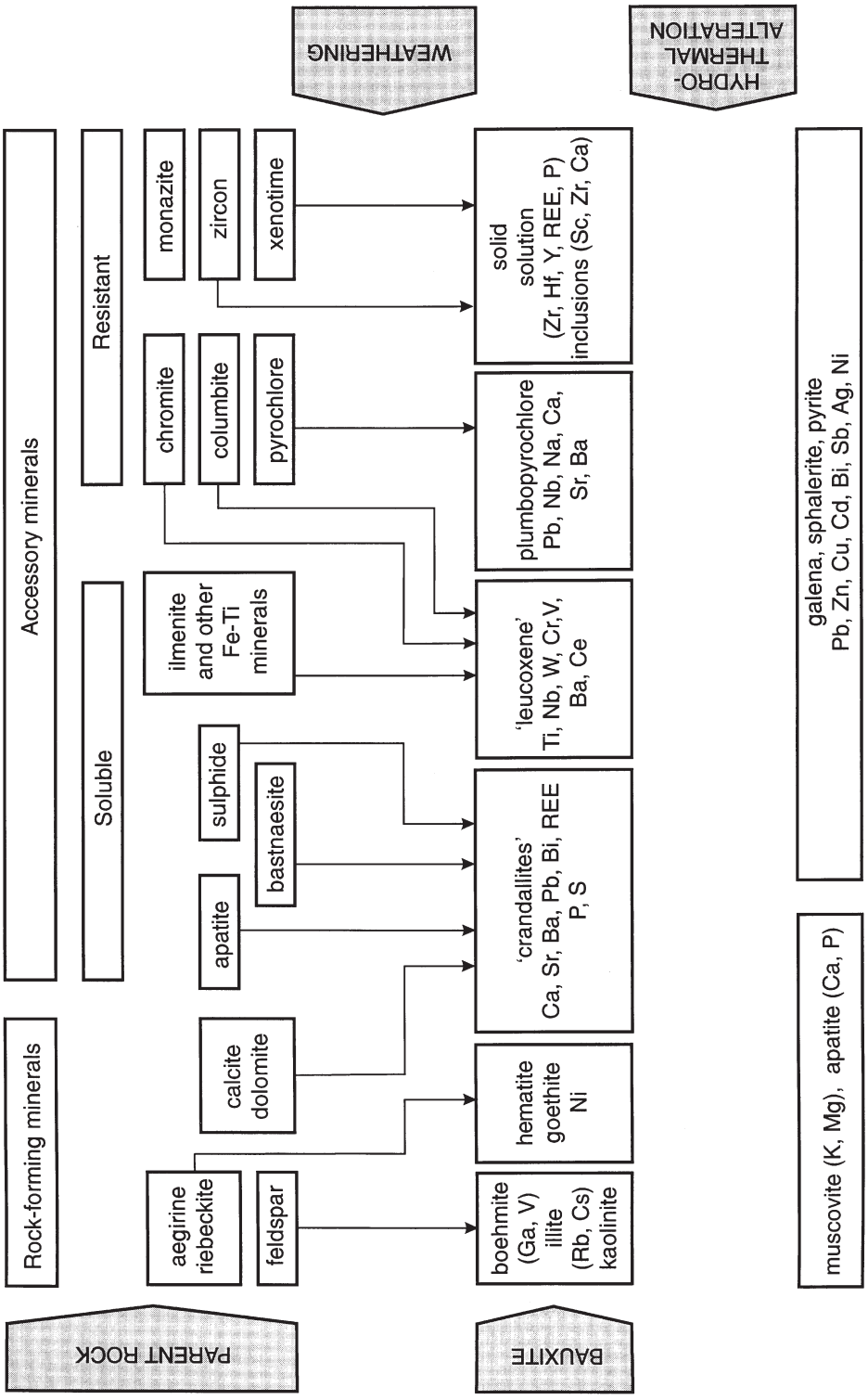

FIG. 14. The scheme of mineral transformation during bauxite weathering and epigenesis.

their formation and alteration can be traced in detail, as most of them show a clear zonal distribution of elements.

While estimating the mobility of an element during bauxite formation, we first have to take into account its mineral forms in both parent rock and weathered profile. Each element demonstrates as many mobilities as there are source minerals in the parent rock. Even the so-called 'immobile' elements such as Ti, Zr, Cr etc. show a certain mobility during bauxite formation and they originate in the rock-forming and soluble accessory minerals. Their mobility is usually restricted within the framework of the weathered sequence.

'Leucoxene' (TiO_2) plays an important role in the accumulation of some elements such as Nb, Cr, W and probably some others. This can explain a positive correlation of Ti with these elements which has been observed in many deposits and frequently used for the identification of a parent rock. Another important mineral is zircon, which may accumulate elements such as Y and P (solid solution), as well as Sc, Ca, Al, Fe and others (inclusions).

Even a very mobile element can lose its mobility in the presence of certain other elements. Thus, the mobility of soluble elements such as Ca, Sr, Ba and Pb can be limited by the presence of P and S which form 'crandallite' group minerals of widely variable composition. The consequence of 'crandallite' growth reflects the rates of dissolution of primary minerals (apatite, galena, bastnaesite etc.).

The studied accessory minerals are known in many bauxite deposits of different origin, which means that the processes of their alteration or formation might be similar to those described above and could be broadly observed within bauxite and laterite profiles.

Acknowledgements

This research was supported by a scholarship from the Alfred Toepfer Foundation F.V.S. (Hamburg) and a Postdoctoral Fellowship from NATO/Royal Society to Dr Leonid Mordberg. Dr C.T. Williams, Mr J. Spratt and Mr F. Galbert performed the high-quality microprobe analyses and produced the X-ray maps, and Mr C. Jones and Dr A. Ball kindly helped obtain the high-resolution photographs.

References

Anderson, R.E. (1971) Notes on the bauxite deposits of Jamaica. *J. Geol. Soc. Jamaica*, *Bauxite Alumina Symp. 1971,* Kingston, 9–16.

Angelica, R.S. and da Costa, M.L. (1993) Geochemistry of Rare-Earth elements in surface lateritic rocks and soils from the Maicuru complex, Para, Brazil. *J. Geochem. Expl*., **47**, 165–82.

Ansheles, O.M. and Vlodavets, N.I. (1927) Strontium mineral from Tikhvin bauxites. *Zap*. *Vses. Min. Obshch.*, **Issue 1**, **Part 56**, 53–60 (in Russian).

Bárdossy, Gy. (1982) *Karst Bauxites. Bauxite Deposits on Carbonate Rocks*. Elsevier, Amsterdam.

Bárdossy, Gy. and Aleva, G.J.J. (1990) *Lateritic Bauxites*. Elsevier, Amsterdam.

Bárdossy, Gy. and Panto, Gy. 1973 Trace element and mineral investigation in bauxites by electron-probe. Pp. 47–54 in: *ICSOBA Troisème Congrès International Nice 1973, Sedal*.

Beneslavsky, S.I. (1974) *Mineralogy of Bauxites* (2nd edition). Nedra, Moscow (in Russian).

Bronevoy, V.A., Zilbermints, V.A. and Teniakov, V.A. (1985) Average chemical composition of bauxites and its evolution in time. *Geokhimia*, **4**, 435–46 (in Russian).

Bulgakova, A.P. (1967) Epigenetic svanbergite in the weathering crust of Lebedinsk deposit, KMA. *Zap. Vses. Min. Obshch.*, **Issue 3**, **Part 96**, 342–5 (in Russian).

Bushinsky, G.I. (1975) *Geology of Bauxites* (2nd edition). Nedra, Moscow.

Dill, H.G., Fricke, A. and Henning, K.H. (1995) The origin of Ba-bearing and REE-bearing aluminium-phosphate-sulphate minerals from the Lohrheim kaolinitic clay deposit (Rheinisches Schiefergebirge, Germany). *Appl. Clay Sci*., **10**, 231–45.

Gaines, R.V., Skinner, H.C.W., Foord, E.E., Mason, B., and Rosenzweig, A. (1997) *Dana's new mineralogy. The system of mineralogy of James Dwight Dana and Edward Salisbury Dana*. John Wiley & Sons Inc., New York.

Germann, K., Fischer, K., Schwarz, T. and Wipki, M. (1995) Distribution and origin of bauxitic laterites in NE-Africa. Pp. 577–80 in: *Mineral Deposits: from their Origin to their Environmental Impacts* (J. Pasava, B. Kribek and K. Zak, editors). Balkema, Rotterdam.

Gomes, C.S.F. (1968) On a Sr and Al basic phosphate-sulphate close to svanbergite occuring in a portuguese bauxitic clay. *Mem. Not. Mus. Lab. Min. Geol. Univ. Coimbra*, **n°** 66, 3–13.

Krumb, J.H. (1998) *Bedingungen, Prozesse und Stoffbilanz der Kaolinisierung – das Beispiel der Lagerstätten Sachsens*. Bodoni, Berlin.

Likhachev, V.V. (1993) Rare-metal bauxite-bearing weathering crust of the Middle Timan. *Komi nauchny tsentr UrO RAN, Syktyvkar* (in Russian).

Lukanina, M.I. (1959) Svanbergite in bauxites of Kamenski District in the Middle Ural. *Zap. Vses. Min. Obshch.,* **Issue 6**, **Part 88**, 586–91 (in Russian).

Makarov, V.N. (1967) Mineral from svanbergite series in the weathering crust of Jakovlevsk deposit, KMA. *Zap. Vses. Min. Obshch*., **Issue 3**, **Part 96**, 342–5 (in Russian).

Maksimović, Z. (1976) Genesis of some Mediterranean karstic bauxite deposits. *Trav. ICSOBA*, **13**, 1–14.

Maksimović, Z. (1979) Geochemical study of the Marmara bauxite deposit: implication for the genesis of brindleyite. *Trav. ICSOBA*, **15**, 121–31.

Maksimović, Z. and Panto, Gy. (1985) Neodymian goyazite in the bauxite deposit of Vlasenica, Yugoslavia. *Tschermaks Min. Petrogr. Mitt.,* **34**, 159–65.

Melfi, A.J., Subies, F., Nahon, D. and Formoso, M.L.L. (1996) Zirconium mobility in bauxites of Southern Brazil. *J. South Amer. Earth Sci.*, **9**: 161–70.

Mordberg, L.E. (1996) Geochemistry of trace elements in Paleozoic bauxite profiles in northern Russia. *J. Geochem. Explor*., **57**, 187–99.

Mordberg, L.E. (1997) Geology, geochemistry and origin of the Schugorsk bauxite deposit, Middle Timan, Russia. *Proc. 8th Int. ICSOBA Congr., Milan, Italy*. *Trav. ICSOBA*, **24**, 35–42.

Mordberg, L.E. (1999) Geochemical evolution of a Devonian diaspore-crandallite-svanbergite-bearing weathering profile in the Middle Timan, Russia. *J. Geochem. Expl*. **66**, 353–61.

Mordberg, L.E., Lyapichev I.G., Furmakova L.N., Panfiltsev D.N. and Dilaktorskaya, E.S. (1997) A model of cesium behaviour in the lateritic weathering of alkaline rocks. *Trans. (Dokl.) Russ. Acad. Sci./Earth Sci. Sect.*, **352**, 145–7.

Mordberg, L.E. and Nesterova, E.N. (1996) Palaeozoic bauxite deposits of North Onega basin (Russia); evidence as to genesis. *Trans. Inst. Mining Metall., Sect. B (Appl. Earth Sci.),* **105**, B200–5.

Mordberg, L.E. and Spratt, J. (1998) Alteration of zircons: the evidence of Zr mobility during bauxitic weathering. *Mineral. Mag.*, **62A**, 1021–2.

Nathan, Y. (1984) The mineralogy and geochemistry of phosphorites. In: *Phosphate Minerals* (J.O. Nriagu and P.B. Moore, editors). Springer-Verlag, Berlin.

Schwab, R.G., Costa, M.L. da and Oliveira, N.P. de. (1983) Über die Entwicklung von Bauxiten und Phosphat-Lateriten der Region Gurupi, Nordbrasilien. *Zentralbl. Geol. Paläont.,* **Teil I**, 563–80.

Schwab, R.G., Herold, H., Costa, M.L. da and Oliveira, N.P. de. (1989) The formation of aluminous phosphates through lateritic weathering of rocks. Pp. 369–86 in: *Weathering; its Products and Deposits* Vol. 2 (A. Barto-Kyriakidis, editor). Theophrastus Publishing & Proprietary Co., S.A. (Ltd.), Athens.

Schwarz, T. and Germann, K. (1999) Weathering surfaces, laterite-derived sediments and associated mineral deposits in north-east Africa. *Spec. Publs. Int. Ass. Sediment*., **27**, 367–90.

Slukin, A.D., Arapova, G.A., Zvezdinskaya, L.V., Tsvetkova, M.V. and Lapin, A.V. (1989) Mineralogy and geochemistry of laterized carbonatites of the USSR. Pp. 171–89 in: *Weathering; its Products and Deposits* Vol. 2 (A. Barto-Kyriakidis, editor). Theophrastus Publishing & Proprietary Co., S.A. (Ltd.), Athens.

Valeton, I. (1972) *Bauxites*. Elsevier, Amsterdam.

Viellard, Ph., Tardy, Y. and Nahon, D. (1979) Stability fields of clays and aluminium phosphates: paragenesis in lateritic weathering of argillaceous phosphatic sediments. *Amer. Mineral.*, **64**, 626–34.

Waber, N., Schorscher, H.D. and Peters, T. (1992) Hydrothermal and supergene uranium mineralization at trhe Osamu Utsumi mine, Minas-Gerais, Brazil. *J. Geochem. Expl*., **45**, 53–112.

Wall, F., Williams, C.T., Woolley, A.R and Nasraoui, M. (1996) Pyrochlore from weathered carbonatite at Lueshe, Zaïre. *Mineral. Mag*., **60**, 731–50.

Wipki, M. (1995) *Eigenschaften, Verbreitung und Entstehung von Kaolinlagerstätten im Nordsudan*. Köster, Berlin.

[*Manuscript received 25 April 1999: revised 22 August 2000*]